LUND UNIVERSITY

Bounds on metamaterials: experimental results

Larsson, Christer; Sohl, Christian; Kristensson, Gerhard; Gustafsson, Mats

2008

[Link to publication](#)

Total number of authors:
4

Bounds on Metamaterials — Experimental Results

Christer Larsson[1,2], Christian Sohl[1], Gerhard Kristensson[1], and Mats Gustafsson[1]

[1]Department of Electrical and Information Technology, Lund University,
P.O. Box 118, S-221 00 Lund, Sweden
[2]Saab Communication, S-581 11 Linköping, Sweden

Abstract— A method to determine the extinction cross section from the monostatic radar cross section is developed and experimentally validated on a fabricated sample of metamaterial. The sample consists of a single-layer planar array of capacitive resonators forming a negative permittivity material. Moreover, a sum rule for the extinction cross section is verified experimentally, and it is concluded that the theory is in good agreement with the measurements in the microwave region.

1. INTRODUCTION

The purpose of this paper is to experimentally verify new theoretical results that bound the scattering from arbitrary objects. These theoretical results have the form of a general sum rule for the extinction cross section, *i.e.*, the sum of the total scattering cross section and the absorption cross section [1, 2]. The sum rule bounds the total amount of electromagnetic scattering and absorption that is available in the entire frequency range. This interesting result needs to be verified experimentally which motivates the present study.

Utilizing the optical theorem it is possible to calculate the extinction cross section from the forward radar cross section (RCS) amplitude [3]. The direct measurement of the forward RCS in free space is experimentally difficult since the largest part of the received field at the receiving antenna consists of a direct illumination by the transmitting antenna. The direct illumination contributes with a dominating background that has to be removed, either using coherent background subtraction or other signal processing methods, from the scattered field.

An additional complication is that RCS measurement ranges are not commonly set up for forward RCS experiments. This is most likely due to the low number of practical applications for forward scattering compared to the monostatic setup. Examples of applications that use scattering in the forward direction are systems for ground target identification [4] and radar fences [5]. A bistatic measurement system where forward scattering can be measured in a laboratory area is described in Ref. 6. It operates in the frequency range $[2, 12.4]$ GHz with a measurement accuracy of ± 1 dB at a level of -18 dBsm in the forward direction. This should be compared to the corresponding results for monostatic RCS at the same measurement range where it is possible to measure down to -50 dBsm with the same accuracy.

In comparison, there are a large number of monostatic radar applications and a wealth of literature treating monostatic RCS measurements [7]. There are even standardized procedures for measuring the monostatic RCS [8]. It is not surprising, considering this, that most free space scattering experiments at indoor and outdoor measurement ranges are setup for monostatic RCS measurements.

Monostatic RCS measurements are therefore to be preferred, compared to forward RCS measurements, if they can be used for the purpose at hand. This paper describes a method to determine the extinction cross section for a thin and non-magnetic planar object over a large bandwidth in the microwave region. The method is based on a conventional measurement of the monostatic RCS and using the fact that the RCS amplitude in the forward and backward directions are equal if the illuminated object is planar and non-magnetic [9, 10]. The monostatic method is compared to and validated with a more general measurement technique based on the RCS in the forward direction.

2. THEORETICAL BACKGROUND

This section gives a short theoretical background to a general sum rule that bounds the scattering from objects. We also define the quantities that are significant for the measurements using RCS notation [7].

Consider the direct scattering of a plane wave $\boldsymbol{E}_0 \mathrm{e}^{\mathrm{i}2\pi\hat{\boldsymbol{k}}\cdot\boldsymbol{r}f/c_0}$ with time dependence $\mathrm{e}^{-\mathrm{i}2\pi ft}$ impinging in the $\hat{\boldsymbol{k}}$-direction on a bounded scatterer embedded in free space (c_0 is the phase velocity of light in free space). The material of the scatterer is modeled by a linear constitutive relation with material parameters that are stationary with respect to time and which satisfies primitive causality and passivity.

The scattering properties in the $\hat{\boldsymbol{r}}$-direction are described for the incident wave polarization $\hat{e}_{\mathrm{i}} = \boldsymbol{E}_0/|\boldsymbol{E}_0|$, scattered electric field $\boldsymbol{E}_{\mathrm{s}}(\boldsymbol{r})$, and polarization of the received wave $\hat{e}_{\mathrm{r}}$ ($\hat{e}_{\mathrm{r}}$ is determined by the receiving antenna). The bistatic RCS amplitude that is recorded in a measurement is then defined as,

$$A(f,\hat{\boldsymbol{r}}) = \frac{2\sqrt{\pi}}{|\boldsymbol{E}_0|} \lim_{r\to\infty} \mathrm{e}^{-\mathrm{i}2\pi fr/c_0} r \boldsymbol{E}_{\mathrm{s}}(\boldsymbol{r}) \cdot \hat{e}_{\mathrm{r}}, \tag{1}$$

where $r = |\boldsymbol{r}|$ denotes the magnitude of the position vector $\boldsymbol{r} = r\hat{\boldsymbol{r}}$. The complex-valued quantity $A(f,\hat{\boldsymbol{r}})$, i.e., the bistatic RCS amplitude, preserves the phase information in the measurement. The bistatic RCS is then defined as

$$\sigma(f,\hat{\boldsymbol{r}}) = |A(f,\hat{\boldsymbol{r}})|^2 = \lim_{r\to\infty} \frac{4\pi}{|\boldsymbol{E}_0|^2} r^2 |\boldsymbol{E}_{\mathrm{s}}(\boldsymbol{r}) \cdot \hat{e}_{\mathrm{r}}|^2, \tag{2}$$

which evaluated in the backward direction, $\hat{\boldsymbol{r}} = -\hat{\boldsymbol{k}}$, produces the familiar expression for the monostatic RCS [7].

The scattering cross section σ_{s} is defined as the scattered power in all directions divided by the incident power flux. It is obtained by averaging $\sigma(f,\hat{\boldsymbol{r}})$ over the unit sphere with respect to $\hat{\boldsymbol{r}}$ for matching polarizations between the scattered wave and the receiving antenna [11],

$$\sigma_{\mathrm{s}}(f) = \frac{1}{4\pi} \iint \sigma(f,\hat{\boldsymbol{r}}) \, \mathrm{dS}. \tag{3}$$

The extinction cross section is defined as the sum of the scattering and absorption cross sections [12],

$$\sigma_{\mathrm{ext}}(f) = \sigma_{\mathrm{s}}(f) + \sigma_{\mathrm{a}}(f), \tag{4}$$

where $\sigma_{\mathrm{a}}(f)$ is a measure of the absorbed power in the scatterer. The extinction cross section is then determined from the scattering in the forward direction, with $\hat{e}_{\mathrm{r}} = \hat{e}_{\mathrm{i}}^*$ and $\hat{\boldsymbol{r}} = \hat{\boldsymbol{k}}$, using the optical theorem [3],

$$\sigma_{\mathrm{ext}}(f) = \frac{c_0}{\sqrt{\pi}f} \mathrm{Im}\, A(f,\hat{\boldsymbol{k}}), \tag{5}$$

where c_0 is the phase velocity of light in free space. Using this notation, the sum rule for the extinction cross section then reads [1, 2],

$$\frac{2}{c_0\sqrt{\pi}} \int_0^\infty \frac{\sigma_{\mathrm{ext}}(f)}{f^2} \, \mathrm{d}f = \lim_{f\to 0} \frac{A(f,\hat{\boldsymbol{k}})}{f^2}. \tag{6}$$

The interpretation of (6) is that there is only a limited amount of scattering and absorption available in the frequency domain and that this amount is bounded from above by the static or low frequency limit of $A(f,\hat{\boldsymbol{k}})/f^2$. The quantity $\lim_{f\to 0} A(f,\hat{\boldsymbol{k}})/f^2$ is proportional to the polarizability dyadics for the scatterer [1, 2].

From the integral representations in Ref. 13 or the discussion in Ref. 11, it follows that for a planar and infinitely thin scatterer subject to a wave incident at normal incidence, the RCS amplitudes in the forward and backward directions, $\hat{\boldsymbol{r}} = \hat{\boldsymbol{k}}$ and $\hat{\boldsymbol{r}} = -\hat{\boldsymbol{k}}$, respectively, are identical, i.e.,

$$A(f,\hat{\boldsymbol{k}}) = A(f,-\hat{\boldsymbol{k}}). \tag{7}$$

Combining (5) and (7) makes it possible to determine σ_{ext} and verify (6) from a measurement of the monostatic RCS amplitude.
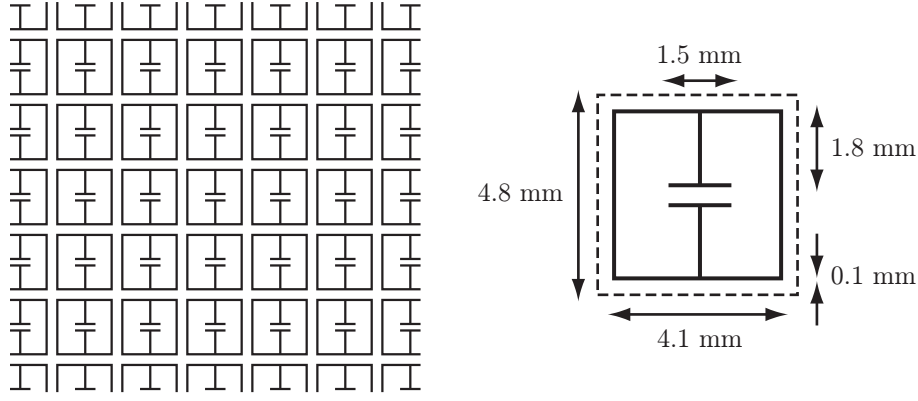
Figure 1: A section of the array of capacitive resonators (left figure) and one unit cell of the array (right figure).

3. EXPERIMENTAL SETUP

The sample design shown in Fig. 1 was used for the experiments. The fabricated single-layer planar array of capacitive resonators is referred to in the literature as a negative permittivity metamaterial [14]. The sample is tuned to be resonant at 8.5 GHz. It consists of 29×29 unit cells supported by a 0.3 mm thick 140 mm $\times$ 140 mm square FR4 substrate, see Fig. 1. The relative dielectric constant, ϵ_{rel}, of the substrate varies between 4.4 and 4.2 in the frequency range $[2, 20]$ GHz with an overall loss tangent less than $5 \cdot 10^{-3}$.

3.1. Monostatic RCS measurements

Monostatic RCS measurements are performed in an anechoic chamber. The sample is mounted on an expanded polystyrene (EPS) sample holder placed on a pylon. The chamber is set up for quasi monostatic RCS measurements with two dual polarized ridged circular waveguide horns positioned at a distance of 3.5 m from the sample, see the left hand side of Fig. 2. The measurement uses an Agilent Performance Network Analyzer (PNA) transmitting a continuous wave without online hard or software gating. The polarizations of the transmitted and received waves are vertical with respect to the pattern in Fig. 1. The original frequency interval $[2, 20]$ GHz is reduced to $[3.2, 19.5]$ GHz due to range (time) domain filtering of the data and a low signal to noise ratio at low frequencies. The latter frequency interval is sampled with 7246 equidistant points corresponding to an unambiguous range of 66.7 m (445 ns). This is sufficient to avoid influence of room reverberations.

Calibration including both amplitude and phase is performed using a metal plate with the same outer dimensions as the sample. A physical optics approximation for a perfectly conducting plate is used as calibration reference [11]. A method of moments calculation for the metal plate is also performed in order to validate the calibration method. The result from this calculation does not deviate significantly from the physical optics approximation. The metal plate is, in addition to being used for calibration, also used to align the experimental setup using the specular reflection from the metal plate. The measured data are processed by a coherent subtraction of the background followed by a calibration. The frequency domain data is then transformed to the range domain, where the response from the sample is selected from the range profile using a 1.1 m spatial gate. Finally, the selected data is transformed back to the frequency domain.

The background subtraction combined with the time gating is sufficient to suppress the background by 15–25 dB. This gives a background level of better than -50 dBsm for the frequency range above 5 GHz and -40 dBsm to -30 dBsm for the lowest part of the frequency range. The high background level at the lower frequencies is a consequence of the wideband horn illumination of the walls at these frequencies. This background level can be maintained for hours by using a single background measurement.

3.2. Forward RCS measurements

Forward RCS measurements are performed using a different setup with ridged waveguide horns in an ordinary laboratory area. The fabricated sample is mounted on an EPS sample holder placed
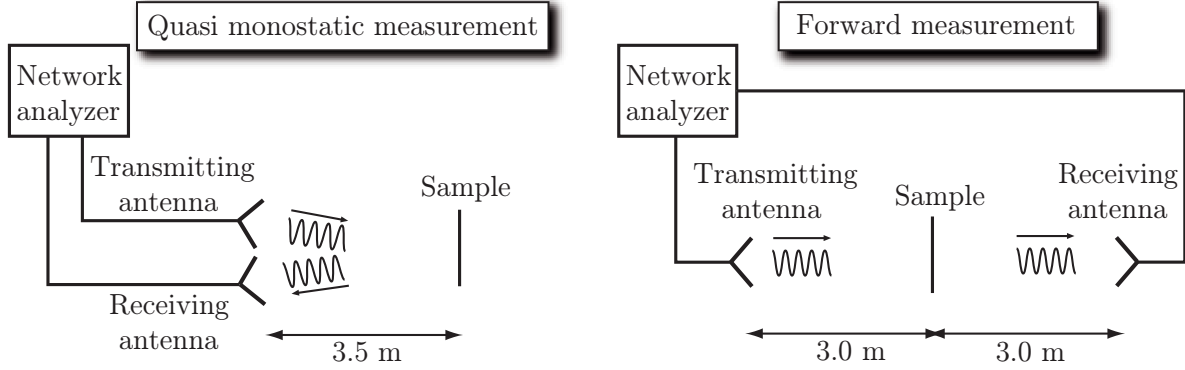
Figure 2: The experimental setups for quasi monostatic (left figure) and forward RCS (right figure) measurements.

on an EPS column. The antennas are positioned facing each other at a distance of 6.0 m with the sample at the midpoint between the antennas, see the right hand side of Fig. 2. In this case an HP 8720C Network Analyzer is used for the measurements with a similar waveform as for the monostatic setup. Four frequency sweeps are interlaced for each measurement in order to obtain 6404 frequency points. The original frequency interval $[1, 18]$ GHz is reduced to $[2.5, 16]$ GHz due to time domain filtering of the data and a low signal to noise ratio at low frequencies. The latter frequency interval is sampled with 5086 equidistant points corresponding to an unambiguous time range of 378 ns. Here we use time units as a measure of the ambiguity range since distance units are less meaningful for forward scattering. The unambiguous time range is sufficient to avoid influence of room reverberations such as delayed scattering from the floor and the walls in the laboratory area.

Calibration including both amplitude and phase is performed using a high precision sphere with radius 6.00 cm. The Mie series for a perfectly electric conducting sphere is used as the calibration reference [11]. A sphere is an ideal calibration object for forward scattering since the sphere is not associated with any alignment problems [6].

The calibration measurement is performed by first measuring the sphere followed by a measurement of the background. The raw data from the calibration is then processed by a coherent subtraction of the background. The Mie series result is divided by the background subtracted calibration data to obtain a calibration vector. The fabricated sample is then measured. A new measurement of the background is coherently subtracted from the sample measurement. The repeated background measurements are important in order to increase the efficiency of the background subtraction and to obtain the background levels mentioned below. We perform the background measurements within less than 2 minutes after each sample (calibration) measurement.

The background subtracted data for the fabricated sample is then calibrated using the calibration vector. The calibrated frequency domain data is transformed to the time domain, where the response from the sample is selected from the time profile using a 1.7 ns time gate. The size of the gate is chosen to minimize the influence from the background. Finally, the selected data is transformed back to the frequency domain. The background subtraction combined with the time gating is sufficient to suppress the background by 50 dB giving a background level of less than -40 dBsm.

4. RESULTS AND DISCUSSION

4.1. Validation of the monostatic method

The left graph in Fig. 3 shows a comparison between measurements of the monostatic RCS and the forward RCS. The agreement is better than 0.5 dB except for the minimum at 10.7 GHz where the discrepancy is 2.5 dB. The measured differences are well within experimental error limits. It is therefore validated that the monostatic RCS and the forward RCS are equal within good accuracy
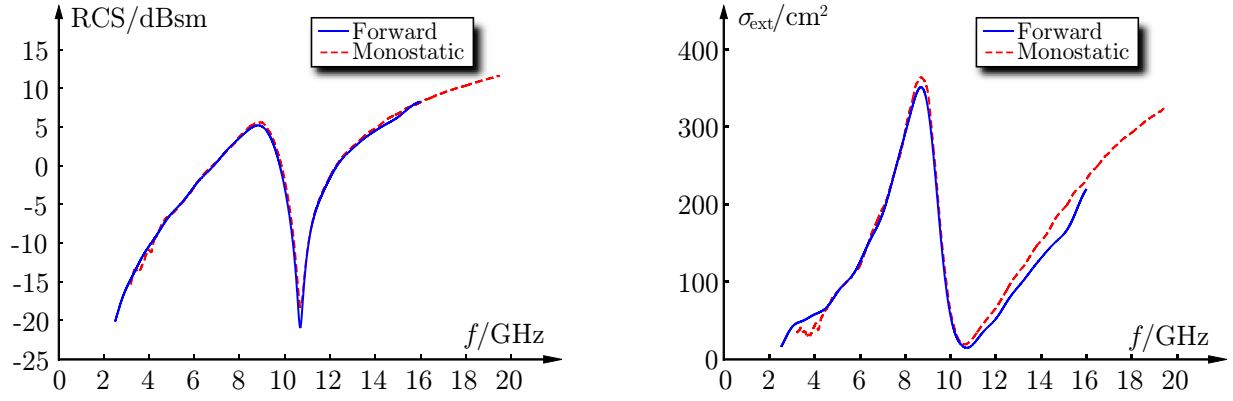
Figure 3: The forward and monostatic RCS (left figure) and the extinction cross section (right figure) determined from the RCS amplitude in the forward and backward directions.

for this thin non-magnetic sample.

However, the phase of the RCS amplitude is also important since the extinction cross section is determined from the imaginary part of the RCS amplitude, see (5). The right part of Fig. 3 shows the extinction cross section determined from (5) using both the monostatic and forward RCS amplitudes. The phase of the forward RCS amplitude is shifted according to the procedure described below in order to compare the two curves. The maximum discrepancy between the curves is $35\,\mathrm{cm}^2$ at $15\,\mathrm{GHz}$ after an adjustment of the phase.

The real and imaginary parts of $A(f,\hat{\boldsymbol{k}})/f^2$ are shown in Fig. 4. The phase of $A(f,\hat{\boldsymbol{k}})/f^2$ obtained from the forward scattering experiment is adjusted using a time delay of $3.1\,\mathrm{ps}$. This adjustment is performed by matching the zero crossings of $\operatorname{Re} A(f,\hat{\boldsymbol{k}})/f^2$ obtained from the forward and monostatic measurements. We believe that the largest contribution to this phase shift is the time delay of the wave as it passes the $0.3\,\mathrm{mm}$ FR4 substrate and the $48\,\mathrm{mm}$ EPS sample support. This delay can also be estimated from the relative dielectric constants of the EPS and FR4 materials. The relative dielectric constant, ϵ_{rel}, for EPS is estimated from the mass density of EPS using Ref. 15. From a mass density of $18.4\,\mathrm{mg/cm}^3$ we obtain $\epsilon_{\mathrm{rel}} = 1.02$ for the EPS material used in the experiment giving a time delay of $1.7\,\mathrm{ps}$. Using $\epsilon_{\mathrm{rel}} = 4.3$ for FR4 yields a corresponding time delay of $1.1\,\mathrm{ps}$ for the FR 4 substrate adding up to a total time delay of $2.8\,\mathrm{ps}$. Small alignment differences between the calibration plate and the fabricated sample in the monostatic case can also account for some of the observed phase difference. The difference between the two measurement methods is small which means that it is validated that conventional monostatic RCS amplitude measurements can be used to determine the extinction cross section for this class of thin and non-magnetic samples.

4.2. Experimental verification of the sum rule (6)

Different methods are used to experimentally verify (6). First the extinction cross section is integrated to obtain a lower bound of $\lim_{f\to 0} A(f,\hat{\boldsymbol{k}})/f^2$. By integrating the measured data in the graph on the right hand side of Fig. 3 the lower bound of $1.1\,\mathrm{cm/GHz}^2$ is obtained using either the forward or the monostatic measurement.

The complex-valued quantity $A(f,\hat{\boldsymbol{k}})/f^2$ can be used to verify that the experimental outcome behaves causally using the Hilbert transform [16]. In Fig. 5, it is observed that the Hilbert transform resembles the overall frequency dependence of the real and imaginary parts of A/f^2. Here the mean values, *i.e.*, the bias, have been removed from both the real and the imaginary parts of $A(f,\hat{\boldsymbol{k}})/f^2$. The figure also shows that the finite frequency interval of the measured data limits the usefulness of the Hilbert transform as a method of reconstructing an unknown component of $A(f,\hat{\boldsymbol{k}})/f^2$.

A possible method to approximate $A(f,\hat{\boldsymbol{k}})/f^2$ is to use a meromorphic function with roots and zeros in the lower half of the complex f-plane. Numerical tests using the algorithm in Ref. 17 indicate that it is sufficient to consider a rational function with a numerator and a denominator of second and fourth degree polynomials, respectively. This function can also be represented by a
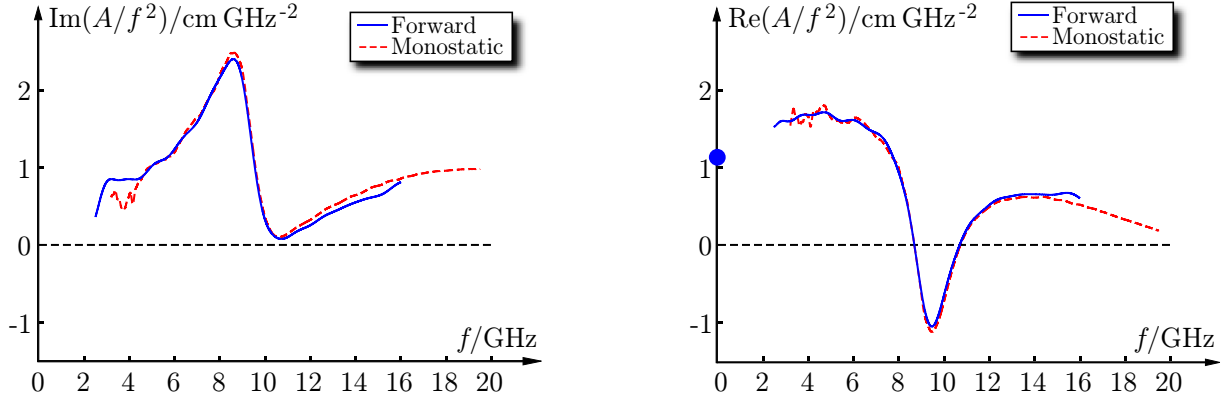
Figure 4: The imaginary part (left figure) and the real part (right figure) of A/f^2 determined from the RCS amplitude in the forward and backward directions. The dot for zero frequency indicates a lower bound of $\lim_{f\to 0} A(f,\hat{\boldsymbol{k}})/f^2$ obtained by integrating the extinction cross section.

sum of two Lorentz resonance models,

$$\frac{A_{\mathrm{appr}}(f,\hat{\boldsymbol{k}})}{f^2} = \sum_{n=1}^{2} a_n \frac{f_n^2 - \mathrm{i}f\nu_n}{f_n^2 - 2\mathrm{i}ff_n/Q_n - f^2}. \tag{8}$$

The optical theorem, (5), can be used to determine an approximation to the extinction cross section, $\sigma_{\mathrm{ext}}^{(\mathrm{appr})}(f)$, from $A_{\mathrm{appr}}(f,\hat{\boldsymbol{k}})$,

$$\sigma_{\mathrm{ext}}^{(\mathrm{appr})}(f) = \frac{\mathrm{c}_0}{\sqrt{\pi}f}\,\mathrm{Im}\,A_{\mathrm{appr}}(f,\hat{\boldsymbol{k}}). \tag{9}$$

The approximation (8) is depicted by the dashed lines in Fig. 6. Here, $f_1 = 9.3\,\mathrm{GHz}$, $Q_1 = 7.8$, $a_1 = 0.2\,\mathrm{cm/GHz}^2$, and $\nu_1 = -27\,\mathrm{GHz}$ for the first term, and $f_2 = 20\,\mathrm{GHz}$, $Q_2 = 1.6$, $a_2 = 1.6\,\mathrm{cm/GHz}^2$, and $\nu_2 = 3.6\,\mathrm{GHz}$ for the second term. In particular, the static limit of (8) is given by $a_1 + a_2 \approx 1.8\,\mathrm{cm/GHz}^2$. It is concluded that the approximations are in good agreement with the experimental results.

A more accurate value for the quantity $\lim_{f\to 0} A(f,\hat{\boldsymbol{k}})/f^2$ on the right hand side of (6) is determined from the approximation in (8). In fact, the lower bound $1.1\,\mathrm{cm/GHz}^2$ obtained by integrating the extinction cross section on the right hand side of Fig. 4 should be compared with the corresponding value $1.5\,\mathrm{cm/GHz}^2$ obtained by integrating $\sigma_{\mathrm{ext}}^{(\mathrm{appr})}(f)$ determined from (9) over the frequency range $[0, 22]\,\mathrm{GHz}$. The lower bound $1.5\,\mathrm{cm/GHz}^2$ is quite close to the static limit $1.8\,\mathrm{cm/GHz}^2$, which is predicted by the parameters in the Lorentz resonance model given above.

5. CONCLUSIONS

We show that monostatic RCS amplitude measurements can be used to determine the extinction cross section for thin and non-magnetic samples by validating the experimental method with a forward RCS measurement. The differences in measured phase can be explained by different path lengths in the two measurements, and the differences in amplitude are well within the experimental error limits. The experimental results show that the sum rule (6) is in good agreement with the measurements. The experimental method to determine the extinction cross section over a large frequency range using a forward scattering technique is currently being refined. With the improved forward technique it is possible to determine the extinction cross section for more general objects. The new work will be reported in a series of forthcoming papers.
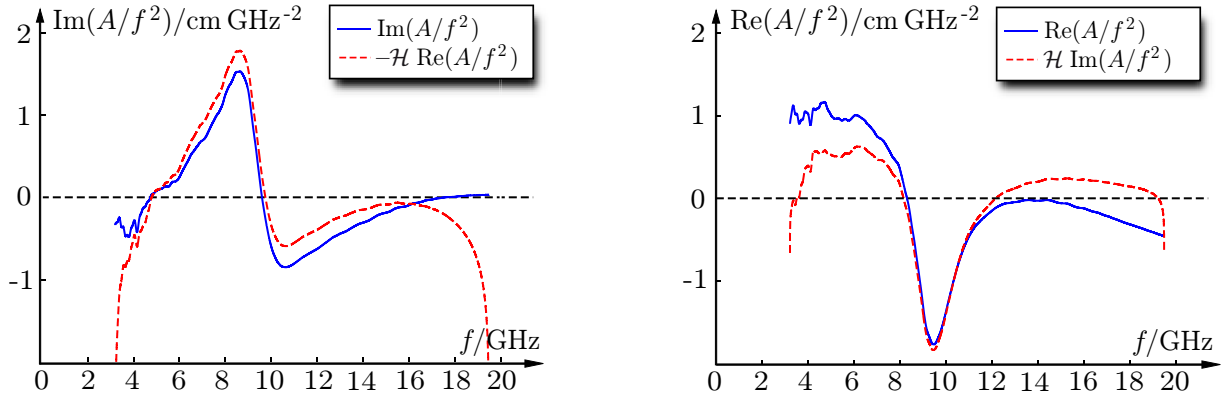
Figure 5: The imaginary (left figure) and real part(right figure) of A/f^2 obtained from monostatic measurements are shown with solid lines. Note that the mean has been removed from both the measured components in this figure. The dashed red lines show the corresponding quantities calculated using the Hilbert transform, $\mathcal{H}$.

Sweden, and in particular Carl-Gustaf Svensson and Mats Andersson for generous hospitality and practical assistance in the measurement campaigns.

REFERENCES

1. C. Sohl, M. Gustafsson, and G. Kristensson. Physical limitations on broadband scattering by heterogeneous obstacles. *J. Phys. A: Math. Theor.*, 40:11165–11182, 2007.
2. C. Sohl, M. Gustafsson, and G. Kristensson. Physical limitations on metamaterials: Restrictions on scattering and absorption over a frequency interval. *J. Phys. D: Applied Phys.*, 40:7146–7151, 2007.
3. R. Newton. Optical theorem and beyond. *Am. J. Phys*, 44:639–642, 1976.
4. M. Cherniakov, R. S. A. R. Abdullah, P. Jancovic, M. Salous, and V. Chapursky. Automatic ground target classification using forward scattering radar. *IEE Proceedings Radar, Sonar and Navigation*, 153(5):427–437, 2006.
5. N. J. Willis. *Bistatic Radar*. Artech House, Boston, London, 1991.
6. M. G. Cote. Automated swept-angle bistatic measurement system. Technical Report RL-TR-93-52, Rome Laboratory, 31 Grenier Street, Hansom AFB MA 01731-3010, 1993. http://stinet.dtic.mil.
7. E. F. Knott, J. F. Shaeffer, and M. T. Tuley. *Radar Cross Section*. SciTech Publishing Inc., 5601 N. Hawthorne Way, Raleigh, NC 27613, 2004.
8. IEEE recommended practice for radar cross-section test procedures, 2007. IEEE Std 1502-2007.
9. C. Sohl, C. Larsson, M. Gustafsson, and G. Kristensson. A scattering and absorption identity for metamaterials: experimental results and comparison with theory. *J. Appl. Phys.*, 103(5):054906, 2008.
10. C. Larsson, C. Sohl, M. Gustafsson, and G. Kristensson. Wideband extinction measurements for thin and planar samples. Technical Report LUTEDX/(TEAT-7166)/1–10/(2008), Lund University, Department of Electrical and Information Technology, P.O. Box 118, S-221 00 Lund, Sweden, 2008. http://www.eit.lth.se.
11. G. T. Ruck, D. E. Barrick, W. D. Stuart, and C. K. Krichbaum. *Radar Cross-Section Handbook*, volume 1 and 2. Plenum Press, New York, 1970.
12. C. F. Bohren and D. R. Huffman. *Absorption and Scattering of Light by Small Particles*. John Wiley & Sons, New York, 1983.
13. S. Ström. Introduction to integral representations and integral equations for time-harmonic acoustic, electromagnetic and elastodynamic wave fields. In V. V. Varadan, A. Lakhtakia, and V. K. Varadan, editors, *Field Representations and Introduction to Scattering*, volume 1 of *Handbook on Acoustic, Electromagnetic and Elastic Wave Scattering*, chapter 2, pages 37–141. Elsevier Science Publishers, Amsterdam, 1991.
14. D. Schurig, J. J. Mock, and D. R. Smith. Electric-field-coupled resonators for negative permittivity metamaterials. *Appl. Phys. Lett.*, 88:041109, 2006.
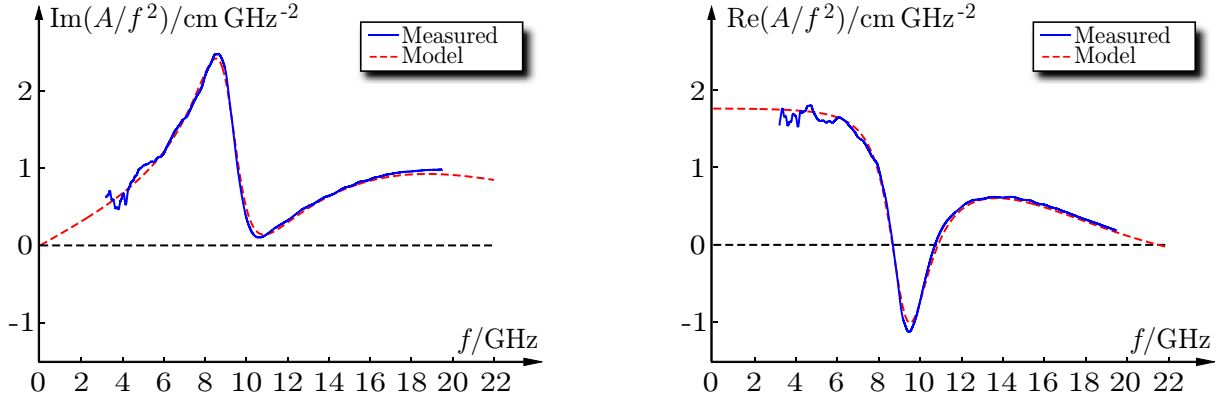
Figure 6: The imaginary (left figure) and real part(right figure) of A/f^2 obtained from monostatic measurements are shown with solid lines. The dashed red lines are given by the model in (8).

15. E. F. Knott. Dielectric constant of plastic foams. *IEEE Trans. Antennas Propagat.*, 41(8):1167–1171, 1993.

16. E. C. Titchmarsh. *Introduction to the Theory of Fourier Integrals.* Oxford University Press, Oxford, second edition, 1948.

17. E. C. Levi. Complex-curve fitting. *IRE Trans. on Automatic Control*, 4:37–44, 1969.